PCCP

PAPER

View Article Online
View Journal | View Issue

Cite this: *Phys. Chem. Chem. Phys.*, 2015, **17**, 10608

Electronic structure of graphene nanoribbons doped with nitrogen atoms: a theoretical insight

A. E. Torres and S. Fomine*

The electronic structure of graphene nanoribbons doped with a graphitic type of nitrogen atoms has been studied using B3LYP, B2PLYP and CAS methods. In all but one case the restricted B3LYP solutions were unstable and the CAS calculations provided evidence for the multiconfigurational nature of the ground state with contributions from two dominant configurations. The relative stability of the doped nanoribbons depends mostly on the mutual position of the dopant atoms and notably less on the position of nitrogen atoms within the nanoribbon. N-graphitic doping affects cationic states much more than anionic ones due the participation of the nitrogen atoms in the stabilization of the positive charge, resulting in a drop in ionization energies (IPs) for N-graphitic doped systems. Nitrogen atoms do not participate in the negative charge stabilization of anionic species and, therefore, the doping does not affect the electron affinities (EAs). The unrestricted B3LYP method is the method of choice for the calculation of IPs and EAs. Restricted B3LYP and B2PLYP produces unreliable results for both IPs and EAs while CAS strongly underestimates the electron affinities. This is also true for the reorganization energies where restricted B3LYP produces qualitatively incorrect results. Doping changes the reorganization energy of the nanoribbons; the hole reorganization energy is generally higher than the corresponding electron reorganization energy due to the participation of nitrogen atoms in the stabilization of the positive charge.

Received 14th January 2015,
Accepted 11th March 2015

DOI: 10.1039/c5cp00227c

www.rsc.org/pccp

Introduction

Recently, graphene has been widely investigated due to its unique physical and electronic properties, since it could represent one of the most promising materials for its implementation in electronic devices.[1,2] It was the research on graphene that unleashed the investigations in the area of graphene nanoribbons. Graphene nanoribbons (GNRs) are graphene strips of nanometric size that, in contrast to their parent structure, were predicted to have a band gap, opening a new field of application in digital electronics.[3] It is inferred that structures fabricated from GNRs (that are just a few nanometres wide) will become key elements for nanoelectronics. Nowadays these structures have been synthesized and they were found to have higher electron mobilities compared to graphene.[4–6]

The properties of GNRs are governed by their geometric parameters and chemical composition. In this regard, the chemical doping is an important strategy for tuning the electronic properties of graphene and the modification the energy gap, similar to that developed for silicon based technology.[7] One of the most employed methods is substitutional doping, where heteroatoms such as nitrogen or boron replace some of the carbon atoms of the sp^2 lattice of graphene. In particular, nitrogen has approximately the same atomic radius as carbon, and has one extra electron, thus modifying its electronic and transport properties.[3,8]

N-doped graphene nanoribbons have recently been studied both experimentally and theoretically. It was found that the nitrogen doping effect depends on the doping site. The most common types of nitrogen in the hexagonal carbon lattice are graphitic, pyridinic and pyrrolic[9–12] (Fig. 1).

It was predicted that N-pyridinic and N-pyrrolic doping of graphene is p-type doping, while graphitic nitrogen induces

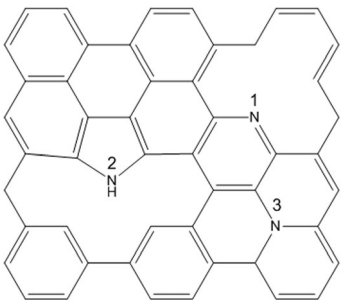

Fig. 1 Nitrogen doping sites in a GNR model structure: pyridinic (1), pyrrolic (2) and graphitic (3).

Universidad Nacional Autónoma de Mexico, Instituto de Investigaciones en Materiales, Mexico, Mexico. E-mail: fomine@unam.mx

n-type conductivity.[8] The assignment of N-pyrrolic doping to the p-type is, however, rather questionable. It is well known that pyrrolic nitrogen is a strong electron-donating group due to the lone pair of the nitrogen atom interacting with the π-electrons of the GNR. Pyrrole itself and related polycyclic heterocycles like carbazole are very reactive towards electrophiles, characteristic of n-doped systems. Moreover, both graphitic and pyrrolic nitrogens have lone pairs and, therefore, should possess similar electron-donating properties.

It has previously been suggested that large aromatic polycyclic hydrocarbons and GNR type structures have ground states possessing multiconfigurational polyradical character.[13–15] On the other hand, it seems that a single reference wavefunction describes well the ground state of polycyclic hydrocarbons when dynamic correlation is properly taken into account.[16–20]

Previously, we have performed a systematic study of the electronic structure of the above mentioned systems. It has been found that the multiconfigurational character of the ground state increases with the size of the system and does not necessarily imply a multiradical character of the ground state found only in very large systems.[21] Therefore, motivated by the previous results we decided to analyze the effect of nitrogen doping on the electronic properties of nanoribbon type structures, taking into account their notable multiconfigurational character, which is important to consider for the correct description of their electronic structure and accurate prediction of their properties.

Computational details

The geometry optimizations were carried out using a D3 dispersion corrected[22] B3LYP functional as implemented in Turbomole 6.6[23] in conjunction with Dunning's correlation consistent cc-pVDZ basis set.[24] The geometries of all the structures were optimized for singlets and triplets using restricted and unrestricted methods, respectively. When triplet instability was detected for the closed shell singlet state, the geometry was reoptimized using a broken symmetry unrestricted method (UB3LYP). Single point energy calculations using a B2PLYP functional[25] were also carried out for the singlet state using restricted and unrestricted reference wavefunctions to study the importance of the nonlocal dynamic correlation.

To evaluate the multiconfigurational character of the studied systems, CAS single point energy calculations were carried out using B3LYP optimized structures of the corresponding multiplicity using active spaces consisting of 10 electrons and 10 orbitals for neutral species, 9 electrons and 10 orbitals for cation radicals and 11 electrons and 10 orbitals for anion radicals. This active space was the largest practical active space possible. For all the atoms the 6-31G(d) 5d basis set[26] was used. All active orbitals were carefully analyzed to ensure that the p electrons of the nitrogen atoms were included in the active space. These calculations were carried out with Gaussian 09 rev. D.01 code.[27] The geometry of the studied GNR is shown in Fig. 2. This GNR has been synthesized experimentally.[28]

The doping effect of graphitic and pyridinic nitrogens has been studied. According to a previous paper[21] the ground state of similar systems possesses a notable multiconfigurational character, with only moderate polyradical character since the most important contributions to the multireference wavefunction come from closed shell singlet configurations.

The graphene nanoribbon model selected to evaluate the nitrogen doping effect has an armchair structure with N (width) = 9, commonly named 9-AGNR. According to the previously reported nomenclature for rectangular polycyclic hydrocarbons[21] of dimensions $\boldsymbol{m} \times \boldsymbol{n}$ where $\boldsymbol{m}$ and $\boldsymbol{n}$ are the number of fused benzene rings in columns and rows, this structure corresponds to a rectangular graphene nanoribbon of 4×6 (R4,6). The amount of nitrogen incorporated in the pristine structure is about 1.4% (atomic; 2 nitrogen atoms) corresponding to the experimental reported values for graphitic doping.[29,30]

The structures of doped graphene nanoribbons are shown in Fig. 2.

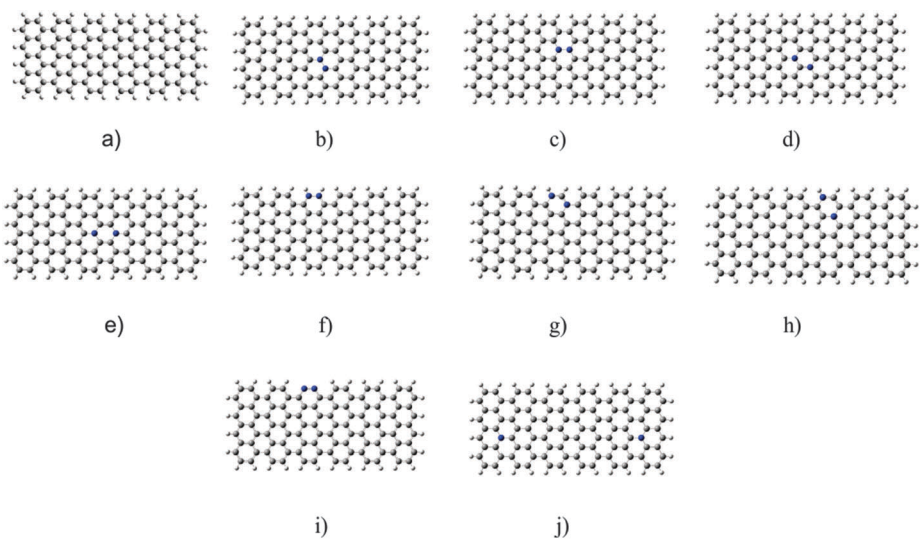

Fig. 2 Pristine (**a**) and core or edge doped graphene nanoribbon structures.

The doping sites for graphitic nitrogen were chosen to cover the maximum number of nonequivalent positions where nitrogen atoms were still interacting with each other. Therefore, the maximum separation between nitrogen atoms was set to 2 carbon atoms. These structures were found to be the most common in nitrogen doped graphene.[31] Moreover, to explore the effect of the doping site type and the separation between doping sites, systems **i** and **j** were also studied. System **i** has pyridinic type doping sites, while in model **j** nitrogen atoms are separated from each other.

The hole reorganization energies (λ_+) of the GNRs were estimated as follows:

$$\lambda_+ = (E_n^+ - E_n) + (E_+^n - E_+)$$

where E_n and E_+ are the energies of the neutral and cationic species in their lowest energy geometries, while E_n^+ and E_+^n are the energies of the neutral and cationic species with the geometries of the cationic and neutral species, respectively. The electron reorganization energy (λ_-) is defined similarly:

$$\lambda_- = (E_n^- - E_n) + (E_-^n - E_-)$$

In this case, E_n and E_- are the energies of the neutral and anionic species in their lowest energy geometries, while E_n^- and E_-^n are the energies of the neutral and anionic species with the geometries of the anionic and neutral species, respectively.

Results and discussion

The relative energies of singlet states calculated for nitrogen doped graphene nanoribbons (N-GNRs) are shown in Table 1. The stability test performed for the restricted B3LYP solutions detected, for all but the neutral specie **j**, triplet instability, therefore, polyradicalic states (PRS) with a multiplicity of 1 were also optimized using UB3LYP. UDFT produces unphysical spin densities since the unrestricted Hamiltonian does not commute with the S^2 operator. However, due to the nature of the broken symmetry unrestricted wavefunction, it describes multireference systems better than a restricted wavefunction does. Following the variational principle, an unrestricted solution is a better approximation to the exact wavefunction since it produces a lower energy state.

The lowest energy structure at the B3LYP level (**j**) was taken as a reference. As seen from Table 1, the order of stability of the structures depends on the method. The best correlation is observed between the UB3LYP and CAS methods, which predict structure **c** to have the highest energy isomers. A similar order of stability was also reported for N-doped graphene sheets.[31] As seen from Table 1, the B2PLYP results are very different from both the CAS and B3LYP results. Given the obtained results it must be noted that *para* N-GNRs are the most energetically stable structures compared with the other N-GNRs. On the other hand, the least stable structures are the *ortho* ones. This is definitely related to the fact that much weaker N–N bonds exist in *ortho* isomers compared to the C–C and C–N bonds of *para* and *meta* doped structures.[32] As seen from the Table 1 the energy difference between isomers reaches various tenths of kcal mol^{-1} for all theory levels. Therefore, the doping topology affects enormously the relative energy of the doped systems. Doping changes the nature of the lowest energy state in two cases at the CAS level. Thus, for structures **b** and **h** the lowest energy state is not a singlet, as for other systems, but a triplet state. In the case of the DFT level of theory, the PRS and triplet states are degenerate within 0.1–0.2 kcal mol^{-1} for all systems.

Table 2 shows the most important configurations contributing to the S0 multireference wavefunction of pristine and doped GNRs. S0 and PRS geometries were used for single point energy evaluation at the CAS/6-31G(d) level. It should be noted that for structures **b** and **h**, S0 is not the ground state according to CAS, and these data are presented here just for comparison purposes. All systems except **j** show clear multireference character. Only for two of the systems, the squared CI expansion coefficient for S0 exceeds 0.46. The RB3LYP solution is stable for system **j**. Therefore it has single reference ground state contributing with only one dominant configuration to the CAS wavefunction.

In all other cases doping with nitrogen atoms does not change the multiconfigurational character of the GNRs, since

Table 1 Relative electronic energies calculated for N-GNRs (kcal mol^{-1}). RB3LYP/cc-pVDZ optimized closed shell singlet (S0) and UB3LYP/cc-pVDZ polyradicalic state (PRS). S0 geometries were used for the single point CAS(10,10)/6-31G(d) (CAS) and B2PLYP/cc-pVDZ calculations

	Relative energy (kcal mol^{-1})			
GNR	S0	CAS	PRS[a]	B2PLYP
b	44.6	40.7[b]	27.0	0.0
c	48.2	56.2	31.2	60.8
d	34.0	50.5	17.1	43.6
e	16.1	18.2	−2.0	22.5
f	18.8	69.4	1.2	26.7
g	22.3	27.4	4.3	40.1
h	7.3	0.0[b]	−9.9	17.1
i	—	—	—	—
j	0.0	28.7	0.0	42.3

[a] The S0 B3LYP energy of structure **j** is taken as the reference for the relative energy calculations at the B3LYP level. [b] The triplet states for these structures are the most stable ones at the CAS level.

Table 2 Squared CI expansion coefficients for the dominant configurations of the GNRs at CAS(10,10)/6-31G(d) level of theory for closed shell singlet (S0) and polyradicalic state (PRS) optimized structures

GNR (S0)	2222200000[a]	2222020000[a]	GNR (PRS)	2222200000[a]	2222020000[a]
a	0.42	0.42	**a**	0.42	0.42
b	0.43	0.43	**b**	0.43	0.43
c	0.32	0.32	**c**	0.32	0.32
d	0.32	0.32	**d**	0.32	0.32
e	0.42	0.42	**e**	0.42	0.42
f	0.84	0.00	**f**	0.41	0.41
g	0.32	0.32	**g**	0.14	0.53
h	0.41	0.41	**h**	0.40	0.40
i	0.46	0.46	**i**	0.45	0.45
j	0.85	0.00	**j**	—	—

[a] Electron distribution in the active orbitals of the dominant configurations.

the most important configurations that appear for the pristine structure are also found in the doped systems contributing to the same extent (two dominant closed shell configurations contribute to the singlet state by over 80%). For systems **c**, **d** and **g**, however, doping promotes the polyradicalic character of the ground state where the contribution of the two above mentioned configurations drops to only 64%; the rest of configurations are polyradicalic (mainly di- and tetra-radicalic). It has been shown[21] that the multiconfigurational character of the electronic state for fused aromatic hydrocarbons decreases with multiplicity. Thus, for systems **b** and **h** where the ground state is triplet, the squared CI expansion coefficients for the dominant triplet configuration are 0.84 and 0.83, respectively, indicating mostly single reference character for these states.

Table 2 demonstrates that there is no significant difference in the dominant configurations of the active space between the closed shell S0 and open shell PRS geometries. The only important variations are for structures **f** and **g** where the geometry choice notably affects the multireference wavefunction.

Table 3 shows the ionization potentials (IPs) and electron affinities (EAs) of the GNRs calculated using different methods.

As can be seen, at the DFT level, the PRS reference state produces notably higher IPs and lower EAs, compared to S0, reflecting the significantly lower total energies of the PRS state compared to the S0 one. According to the DFT results, N-graphitic doping leads to a drop in IP, while pyridinic nitrogens increase the IP (model **i**). The most pronounced decrease in the IP was detected for the *meta* (**d**) structure. Since no experimental data are available for the IPs of GNRs we were only able to compare the calculated IPs with the graphene work function (4.3 eV[33]). As can be seen, the graphene work function is very close to the calculated IP for the pristine GNR (**a**) estimated with a restricted S0 state as a reference state (4.43 eV). It is well known, however, that IPs of conjugated systems drop with the number of atoms involved in the conjugation.

Therefore, the use of a restricted S0 state as the reference state for IPs definitely underestimates the IP for GNR **a**. IP estimations using CAS must be much closer to the real values, since it has been shown that CAS produces IPs for conjugated hydrocarbons only several tenths of an eV higher than experimental values.[34] According to CAS, the IP of pristine GNR (**a**) is 5.75 eV, while UB3LYP predicts a value of 5.19 eV. Considering the above it seems that the UB3LYP method gives a reasonable estimation of IP in spite of strong spin contamination existing in the neutral state ($\langle S^2 \rangle$ = 2.11, Table 5) compared to the restricted B3LYP method.

The overestimation of the neutral state energy, taking place for the restricted B3LYP method will lead also to the overestimation of EA. As seen, EAs calculated using a restricted S0 energy as a reference is almost 1 eV higher compared to these calculated with a PRS state.

Moreover, anion radicals have a low spin contamination (Table 5) which produces more reliable EAs for the studied systems. CAS however, strongly underestimates EAs due to a significant difference in dynamic correlation between the neutral and anionic state[35] predicting a positive electron affinity for most of the studied systems. B2PLYP produces very high and unreliable IPs in most of the cases and positive or weakly negative EAs. This is probably related to the lack of static correlation in this method and the low ''quality'' of the closed shell reference wavefunction.

IPs are the most affected by doping, while EAs barely change when carbons are replaced by nitrogens. EAs slightly decrease in the case of graphitic doping and increase for pyridinic doped system **i**. This is due to the fact that the lone electron of the graphitic nitrogen is relatively weakly bound, decreasing the IP of the doped system. As an example, Fig. 2 shows that the unpaired spin density distribution in the cation radical of structure **d** involves 2 nitrogen atoms, whereas no nitrogen atoms are involved in anion radical stabilization.

Table 4 shows the contributions of the dominant configurations to the multiconfigurational wavefunction of the cation and anion radicals obtained from the CAS calculations and the difference in natural charges for the nitrogen atoms between the neutral and charged N-GNRs. Unlike neutral GNRs, most of the charged systems can be described with only one dominant configuration except for **g+** where the dominant configuration contributes by only 32%. For some of the positively charged N-GNRs, the dominant configuration is polyradicalic as seen for cation radicals **c**, **f**, **g** and **h**. All anion radicals are, however, well described by only one configuration with an unpaired electron. This difference can also be seen from Table 5 where

Table 3 Adiabatic ionization potentials (IP) and electron affinities (EA) estimated at the CAS(10,10)/6-31G(d) (CAS), B2PLYP/cc-pVDZ (B2PLYP), RB3LYP/cc-pVDZ (S0) and UB3LYP/cc-pVDZ (PRS) levels (eV)

GNR	IP S0 (eV)	IP PRS (eV)	IP CAS[a] (eV)	IP B2PLYP[a] (eV)	EA S0 (eV)	EA PRS (eV)	EA CAS[a] (eV)	EA B2PLYP[a] (eV)
a	4.43	5.19	5.75	6.68	−2.90	−2.13	0.37	0.08
b	3.89	4.65	6.38[b]	9.19	−2.83	−2.07	0.63[b]	2.12
c	3.76	4.49	3.63	6.07	−2.85	−2.11	1.11	−1.03
d	3.54	4.27	6.04	6.65	−2.82	−2.08	0.92	−0.31
e	3.96	4.74	6.22	6.39	−2.84	−2.06	0.76	−0.78
f	3.92	4.68	4.19	6.83	−2.85	−2.08	−1.20	0.17
g	3.61	4.39	3.96	5.42	−2.82	−2.04	0.42	−0.56
h	3.84	4.58	6.25[b]	6.13	−2.84	−2.09	0.39[b]	−0.27
i	4.51	5.27	5.92	4.79	−2.96	−2.19	0.41	−2.75
j	4.55	—	5.94	5.61	−2.10	—	0.06	−1.55

[a] RB3LYP/cc-pVDZ and UB3LYP/cc-pVDZ geometries were used for the calculations of the neutral molecule and cation, respectively. [b] The triplet state was taken as a reference for the neutral structure.

Table 4 Squared CI expansion coefficients for the dominant configurations in the cation (C_+^2) and anion radicals (C_-^2) at CAS(9,10)/6-31G(d) and CAS(11,10) levels of theory. The difference in natural charges for the nitrogen atoms between the cationic and neutral (Δ^+) and anionic and neutral (Δ^-) states at the UB3LYP/cc-pVDZ level of theory are shown

Molecule	C_+^2	Configuration	Δ^+	C_-^2	Configuration	Δ^-
a	0.94	2222a00000[a]	—	0.94	222220a000[a]	—
b	0.98	2222a00000[a]	0.100	0.94	22222a0000[a]	−0.006
c	0.94	a2220ab000[a]	0.119	0.98	222a220000[a]	−0.005
d	0.98	2222a00000[a]	0.015	0.98	22222a0000[a]	−0.003
e	0.98	2222a00000[a]	0.102	0.98	222220a000[a]	−0.008
f	0.96	a22200b00a[a]	0.145	0.98	22222a0000[a]	−0.010
g	0.34	2a2abab000[a]	0.050	0.90	22222a0000[a]	0.000
h	0.94	a2220ab000[a]	0.139	0.92	222220a000[a]	−0.009
i	1.00	2222a00000[a]	0.014	1.00	22222a0000[a]	−0.015
j	1.00	2222a00000[a]	0.004	0.90	22222a0000[a]	−0.03

[a] Electron distribution in active orbitals of dominant configurations.

Table 5 $\langle S^2 \rangle$ expectation values for the GNRs for neutral (NEU), cationic (CAT) and anionic (ANI) species at the B3LYP/cc-pVDZ level

GNR	NEU	CAT	ANI
a	2.11	0.80	0.78
b	1.11	1.86	0.79
c	1.22	1.86	0.79
d	1.52	1.91	0.94
e	1.11	1.84	0.79
f	1.16	1.87	0.79
g	2.08	1.85	1.59
h	1.12	1.86	0.79
i	1.12	0.79	0.79
j	0.00	0.83	0.77

$\langle S^2 \rangle$ expectation values are listed for the neutral, cationic and anionic species of the GNRs calculated at the UB3LYP level. The spin contamination for the cation radicals of graphitic doped GNRs is always higher than that for the corresponding anion radicals, indicating a higher polyradicalic character of the cationic species. This difference resides in the character of the delocalization of the polarons in the cation and anion radicals. Fig. 3 shows a typical case where the electrons of the nitrogen atoms participate in the stabilization of the cation radicals but not the anion radicals. This increases the polyradicalic character of the cation radicals compared to the anion radicals, which also reflects the increased spin contamination of the doped cation radicals compared to the anion radicals in the case of graphitic doping (Table 5). It is noteworthy that for pristine structure **a** the spin contamination is small and similar for both cation and anion radicals, thus demonstrating the effect of graphitic nitrogen doping on the polyradicalic character of the cation radicals of N-GNRs. A similar conclusion can be made from analyzing the charge differences on the nitrogen atoms between cationic, neutral and anionic states. As seen from Table 4, the charges on the nitrogen atoms are practically the same in the neutral and anionic state, while in the case of the cations, nitrogen atoms participate actively in the stabilization of the positive charge. Thus, in the case of **h+** some 14% of the positive charge is located on only two nitrogen atoms while the rest of the positive charge is delocalized over the remaining

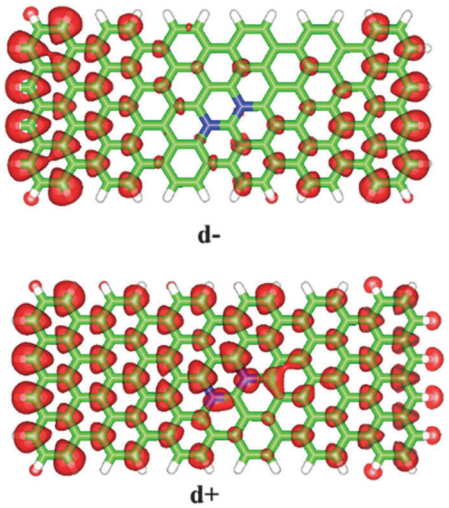

Fig. 3 Spin density distribution in the anion and cation radicals for structure **d**.

106 carbons of the N-GNR. In the case of pyridinic type doping, nitrogen atoms do not participate in the stabilization of the positive charge in the cation radicals as follows from Table 4.

An important step in understanding the conductivity of doped GNRs is to characterize the structural factors which affect charge transfer rates. Thus, it has been demonstrated that the solid-state hole mobility in arylamines is related to the internal reorganization energy. Low internal reorganization energies of isolated molecules have been associated with higher solid-state charge carrier mobility (when combined with large electronic coupling) critical for the development of high efficiency electronic devices. It is known that most organic semiconductors have internal reorganization energies greater than 0.1 eV. Interestingly, several p-type organic semiconductors have been reported with internal reorganization energies (λ_+) of less than 0.1 eV. However, only a few π-type acceptors with electron reorganization energies (λ_-) of less than 0.1 eV, including fullerene C_{60} (0.060 eV), are known.[36] The reorganization energy decreases with increasingly large conjugated cores; for example, for triphenylene it is 0.18 eV, for coronene 0.13 eV and for hexa-peri-hexabenzocoronene 0.1 eV.[37–39]

The charge transport mechanism in GNRs depends on their size. Thus, in the case of a large GNR (40 nm wide) the ballistic mechanism is operational.[5] However, for smaller systems all experimental data point to a hopping mechanism.[40]

Table 6 summarizes calculated λ_+ and λ_- values for pristine and doped GNRs. Since the closed shell singlet solution is not stable for neutral GNRs at the B3LYP level due to the multiconfigurational character of the ground state, the UB3LYP method along with the RB3LYP method were used for the calculations of the E_n, E_n^- and E_n^+ energies. The RB3LYP method produced converged solutions only for systems **b**, **g** and **h**. To the best of our knowledge there is no available experimental data on the reorganization energy of pristine or doped GNRs. However, it is reasonable to suggest that the reorganization energies of pristine GNR must be of the order of 0.1 eV or less.

Table 6 Reorganization energies for electrons (λ_-) and holes (λ_+) (eV) estimated using the UB3LYP and RB3LYP methods, respectively, for the neutral species

	UB3LYP/cc-pVDZ		RB3LYP/cc-pVDZ	
GNR	λ_+ (eV)	λ_- (eV)	λ_+ (eV)	λ_- (eV)
a	0.021	0.020	—[a]	—[a]
b	0.274	0.004	0.010	0.317
c	0.104	0.009	—[a]	—[a]
d	0.335	0.330	—[a]	—[a]
e	0.077	0.002	—[a]	—[a]
f	0.101	0.037	—[a]	—[a]
g	0.248	0.201	0.063	−0.567
h	0.060	0.037	0.022	0.026
i	0.029	0.029	—[a]	—[a]
j	—	—	0.011	0.010

[a] SCF not converged.

Moreover, it has been demonstrated that the B3LYP functional used for the reorganization energy calculations best reproduces the experimental data for the organic conjugated systems.[41,42] As seen from Table 6, the RB3LYP method delivers unreliable reorganization energies (negative λ_- for doped system **g**). Random errors are introduced to the reorganization energy data due to unstable restricted solutions for the E_n, E_n^- and E_n^+ energy calculations. Moreover, for most of the cases RB3LYP did not deliver converged solutions. The UB3LYP method, on the other hand, gives physically meaningful results as seen from Table 6. Very small and similar λ_- and λ_+ values were calculated for pristine system **a**. Nitrogen doping notably affects the reorganization energies. Thus, doping in the *meta* position (structures **d** and **g**) significantly increases both λ_- and λ_+. Systems **b**, **c** and **f**, where nitrogen atoms are in the *ortho* position, forming an explicit covalent bond between them, show an increase in λ_+, while the value of λ_- remains very small. The reorganization energies of **e** and **h**, where nitrogen atoms are *para* to each other are affected less by doping compared to all other structures. As seen from Table 6 the relative position of the nitrogen atoms more greatly affects the reorganization energy than their position within the GNR (core or edge). For the most stable structure **j** the reorganization energy is only slightly higher than that for pristine GNR, remaining notably low.

Conclusions

The relative stability of N-GNRs is strongly related to the mutual position of the dopant atoms and much less with the position of the nitrogen atoms within the nanoribbon. Doping does affect the multireference character of the N-GNR in their neutral state. Thus, for model **j**, where nitrogen atoms are well separated from each other, the ground state is a single reference. In spite of the significant multiconfigurational character detected for most of the singlet ground states, GNRs only exhibited two dominant closed shell singlet configurations. For the ionic species this is not the case and single reference methods give a reasonable description. As a result the single reference method does not provide a well balanced description for both structures, thus giving too low IPs and too high EAs.

Graphitic nitrogen doping more greatly affects the cationic states compared to anionic ones due to the participation of the nitrogen atoms in the stabilization of the positive charge. This results in a drop in IP of the N-GNR. On the other hand nitrogen atoms do not participate in the negative charge stabilization of anionic species, and thus do not affect the EAs of N-GNRs. This is not the case for pyridinic doping (model **i**) where doping results in an increase in IP and EA and, therefore, can be considered as p-doping, unlike n-doping caused by graphitic nitrogen.

The UB3LYP method is the method of choice for the calculation of IPs and EAs. The restricted B3LYP method produces unreliable results for both IPs and EAs while CAS strongly underestimates the electron affinities. This shortcoming of CAS could definitely be repaired using a perturbative correction to the CAS energy. However, the computational cost of this correction is prohibitively high to implement for such large systems. B2PLYP overestimates the IPs and underestimates the EAs of GNRs probably due to the low "quality" of the closed shell reference wavefunction and lack of static correlation. A similar observation is also true for the reorganization energies where the restricted B3LYP method produces qualitatively incorrect results, while UB3LYP delivers the results which are in line with those estimated for known organic conjugated systems. The doping changes the reorganization energy of the N-GNRs; λ_+ being always higher than the corresponding λ_- for graphitic type doping due to the participation of nitrogen atoms in the stabilization of the positive charge.

Acknowledgements

We acknowledge financial support from the Program to Support Research and Technological Innovation Projects (PAPIIT) (grant IN-IN100215) and we would also like to thank the General Direction of Computing and Information Technologies and Communication of the National Autonomous University of Mexico (DGTIC-UNAM) for the support to use the supercomputer facilities. A. E. Torres gratefully acknowledges Consejo Nacional de Ciencia y Tecnología (CONACyT) for a graduate scholarship (245467).

References

1 A. K. Geim and K. S. Novoselov, *Nat. Mater.*, 2007, **6**, 183.
2 A. H. Castro Neto, F. Guinea, N. M. R. Peres, K. S. Novoselov and A. K. Geim, *Rev. Mod. Phys.*, 2009, **81**, 109.
3 T. H. Vo, M. Shekhirev, D. A. Kunkel, M. D. Morton, E. Berglund, L. Kong, P. M. Wilson, P. A. Dowben, A. Ender and A. Sinitskii, *Nat. Commun.*, 2014, **5**, 3189.
4 J. Cai, P. Ruffieux, R. Jaafar, M. Bieri, T. Braun, S. Blankenburg, M. Muoth, A. P. Seitsonen, M. Saleh, X. Feng, K. Müllen and R. Fasel, *Nature*, 2010, **466**, 470.

5 J. Baringhaus, M. Ruan, F. Edler, A. Tejeda, M. Sicot, A. Taleb-Ibrahimi, A. Li, Z. Zhigang Jiang, E. H. Conrad, C. Berger, C. Tegenkamp and W. A. de Heer, *Nature*, 2014, **506**, 349.
6 L. A. Chernozatonskii, P. B. Sorokin and A. A. Artukh, *Russ. Chem. Rev.*, 2014, **83**, 251.
7 D. Usachov, O. Vilkov, A. Grüneis, D. Haberer, A. Fedorov, V. K. Adamchuk, A. B. Preobrajenski, P. Dudin, A. Barinov, M. Oehzel, C. Laubschat and D. V. Vyalikh, *Nano Lett.*, 2011, **11**, 5401.
8 D. Y. Usachov, A. V. Fedorov, O. Y. Vilkov, B. V. Senkovskiy, V. K. Adamchuk, B. V. Andryushechkin and D. V. Vyalikh, *Phys. Solid State*, 2013, **55**, 1325.
9 R. Peköz and S. Erkoc, *Physica E*, 2009, **42**, 110.
10 J. Zeng, K. Q. Chen, J. He, Z. Q. Fan and X. J. Zhang, *J. Appl. Phys.*, 2011, **109**, 124502.
11 S. S. Chauhan, P. Srivastava and A. K. Shrivastava, *Appl. Nanosci.*, 2014, **4**, 461.
12 T. H. Vo, M. Shekhirev, D. A. Kunkel, F. Orange, M. J.-F. Guinel, A. Enders and A. Sinitskii, *Chem. Commun.*, 2014, **50**, 4172.
13 M. Bendikov, H. M. Duong, K. Starkey, K. N. Houk, E. A. Carter and F. Wudl, *J. Am. Chem. Soc.*, 2004, **126**, 7416.
14 D. Jiang and S. J. Dai, *J. Phys. Chem. A*, 2008, **112**, 332.
15 F. Plasser, H. Pašalić, M. H. Gerzabek, F. Libisch, R. Reiter, J. Burgdörfer, T. Müller, R. Shepard and H. Lischka, *Angew. Chem., Int. Ed.*, 2013, **52**, 2581.
16 B. Hajgato, D. Szieberth, P. Geerlings, F. De Proft and M. S. Deleuze, *J. Chem. Phys.*, 2009, **131**, 224321.
17 B. Hajgato, M. Huzak and M. S. Deleuze, *J. Phys. Chem. A*, 2011, **115**, 9282.
18 M. Huzak, M. S. Deleuze and B. Hajgato, *J. Chem. Phys.*, 2011, **135**, 104704.
19 B. Hajgató and M. S. Deleuze, *Chem. Phys. Lett.*, 2012, **553**, 6.
20 M. S. Deleuze, M. Huzak and B. Hajgató, *J. Mol. Model.*, 2013, **417**, 17.
21 A. E. Torres, P. Guadarrama and S. Fomine, *J. Mol. Model.*, 2014, **20**, 2208.
22 S. Grimme, J. Antony, S. Ehrlich and H. Krieg, *J. Chem. Phys.*, 2010, **132**, 154104.
23 TURBOMOLE V6.5 2013, a development of University of Karlsruhe and Forschungszentrum Karlsruhe GmbH, 1989–2007, TURBOMOLE GmbH, since 2007, available from http://www.turbomole.com.
24 T. H. Dunning Jr., *J. Chem. Phys.*, 1989, **90**, 1007.
25 S. Grimme, *J. Chem. Phys.*, 2006, **124**, 034108.
26 R. Ditchfield, W. J. Hehre and J. Pople, *J. Chem. Phys.*, 1971, **54**, 724.
27 M. J. Frisch, *et al.*, *Gaussian 09, revision D.01*, Gaussian Inc, Wallingford, 2013.
28 J. Cai, P. Ruffieux, R. Jaafar, M. Bieri, T. Braun, S. Blankenburg, M. Muoth, A. P. Seitsonen, M. Saleh, X. Feng, K. Müllen and R. Fasel, *Nature*, 2010, **466**, 470.
29 D. Usachov, O. Vilkov, A. Grüneis, D. Haberer, A. Fedorov, V. K. Adamchuk, A. B. Preobrajenski, P. Dudin, A. Barinov, M. Oehzelt, C. Laubschat and D. V. Vyalikh, *Nano Lett.*, 2011, **11**, 5401.
30 H. Wang, T. Maiyalagan and X. Wang, *ACS Catal.*, 2012, **2**, 781.
31 R. Lv, Q. Li, A. R. Botello-Méndez, T. Hayashi, B. Wang, A. Berkdemir, Q. Hao, A. L. Elías, R. Cruz-Silva, H. R. Gutiérrez, Y. A. Kim, H. Muramatsu, J. Zhu, M. Endo, H. Terrones, J.-C. Charlier, M. Pan and M. Terrones, *Sci. Rep.*, 2012, **2**, 586.
32 Y.-R. Luo, *Comprehensive Handbook of Chemical Bond Energies*, CRC Press, Boca Raton, FL, 2007.
33 H. Hibino, H. Kageshima, M. Kotsugi, F. Maeda, F.-Z. Guo and Y. Watanabe, *Phys. Rev. B: Condens. Matter Mater. Phys.*, 2009, **79**, 125437.
34 A. Rehaman, M. Shahi, C. J. Cramer and L. Gagliardi, *Phys. Chem. Chem. Phys.*, 2009, **11**, 10964.
35 R. González-Luque, M. Merchfin, P. Borowski and B. O. Roos, *Theor. Chim. Acta*, 1993, **86**, 467.
36 W. Senevirathna, C. M. Daddario and G. Sauvé, *J. Phys. Chem. Lett.*, 2014, **5**, 935.
37 B. C. Lin, C. P. Cheng and Z. P. M. Lao, *J. Phys. Chem. A*, 2003, **107**, 5241.
38 M. Malagoli and J. L. Brédas, *Chem. Phys. Lett.*, 2000, **327**, 13.
39 K. Sakanoue, M. Motoda, M. Sugimoto and S. Sakaki, *J. Phys. Chem. A*, 1999, **103**, 5551.
40 M. Y. Han, J. C. Brant and P. Kim, *Phys. Rev. Lett.*, 2010, **104**, 056801.
41 N. E. Gruhn, D. A. da Silva, T. G. Bill, M. Malagoli, V. Coropceanu, A. Kahn and J. L. Brédas, *J. Am. Chem. Soc.*, 2002, **124**, 7918.
42 X. Amashukeli, J. R. Winkler, H. B. Gray, N. E. Gruhn and D. L. Lichtenberger, *J. Phys. Chem. A*, 2002, **106**, 7593.

